The statistical parton distributions: status and prospects

Claude Bourrely and Jacques Soffer

Centre de Physique Théorique, UMR 6207 [1],
CNRS-Luminy, Case 907
F-13288 Marseille Cedex 9 - France

Franco Buccella

Dipartimento di Scienze Fisiche, Università di Napoli,
Via Cintia, I-80126, Napoli and INFN, Sezione di Napoli, Italy

Abstract

New experimental results on polarized structure functions, cross sections for $e^{\pm}p$ neutral and charge current reactions and ν ($\bar{\nu}$) charge current on isoscalar targets are compared with predictions using the statistical parton distributions, which were previously determined. New data on cross sections for Drell-Yan processes, single jet in $p\bar{p}$ collisions and inclusive π^0 production in pp collisions are also compared with predictions from this theoretical approach. The good agreement which we find with all these tests against experiment, strenghtens our opinion on the relevance of the role of quantum statistics for parton distributions. We will also discuss the prospects of this physical framework.

---

[1]UMR 6207 - Unité Mixte de Recherche du CNRS et des Universités Aix-Marseille I, Aix-Marseille II et de l'Université du Sud Toulon-Var - Laboratoire affilié la FRUMAM

1 Introduction

Deep-inelastic scattering (DIS) of leptons and nucleons is, so far, our main source of information to study the internal nucleon structure, in terms of parton distributions. Three years ago we proposed [1] to construct, in a unique way, the unpolarized and the polarized parton distributions, using a simple procedure, inspired by a quantum statistical picture of the nucleon, in terms of Fermi-Dirac and Bose-Einstein functions. An important feature of this new approach lies into the fact that the chiral properties of perturbative quantum chromodynamics (QCD), lead to strong relations between quark and antiquark distributions. As a consequence the determination of the best known unpolarized light quarks (u, d) distributions and their corresponding polarized ones $(\Delta u, \Delta d)$, allows to predict the light antiquarks distributions $(\bar{u}, \bar{d}, \Delta \bar{u}, \Delta \bar{d})$. Therefore our approach has a strong predictive power, in particular, the flavor-asymmetric light sea, *i.e.* $\bar{d} > \bar{u}$, which can be understood in terms of the Pauli exclusion principle, based on the fact that the proton contains two u quarks and only one d quark [2]. It is also natural to anticipate that the signs of $\Delta \bar{u}$ and $\Delta \bar{d}$ are the same as Δu and Δd, respectively. One more relevant point to recall, is that all these parton distributions were determined in terms of only *eight* free parameters, which is indeed remarkable.

More recently we compared [3] our predictions with some new unpolarized and polarized DIS measurements obtained at DESY, SLAC and Jefferson Lab. and they turned out to be rather satisfactory. Therefore, in order to strengthen the relevance of this physical picture, we carry on the comparison with data from a much broader set of processes, including new DIS results and also hadronic cross sections.

The paper is organized as follows. In the next section, we review the main points of our approach for the construction of the statistical parton distributions and we recall their explicit expressions. In section 3, we discuss in more details the predictive power of our approach in connection with some simple mathematical properties of the Fermi-Dirac expressions and the numerical values we found for the free parameters. It allows us to clarify the x behavior of the quark distributions, where it is known from the data, but also to foresee some specific behaviors, in so far unexplored regions, for example in the high x domain. In section 4, we consider $e^{\pm}p$ neutral and charged current reactions, whereas section 5 deals with $\nu(\bar{\nu})p$ charged current reactions. Section 6 concerns Drell-Yan processes, while section 7 deals with

inclusive single-jet production in $p\bar{p}$ collisions and inclusive π^0 production in pp collisions. We give our final remarks and conclusions in the last section.

2 The quantum statistical parton distributions

The light quarks $q = u, d$ of helicity $h = \pm$, at the input energy scale $Q_0^2 = 4\text{GeV}^2$, are given by the sum of two terms [1], a quasi Fermi-Dirac function and a helicity independent diffractive contribution, common to all light quarks

$$xq^h(x, Q_0^2) = \frac{AX_{0q}^h x^b}{\exp[(x - X_{0q}^h)/\bar{x}] + 1} + \frac{\tilde{A}x^{\tilde{b}}}{\exp(x/\bar{x}) + 1} \ . \tag{1}$$

Here X_{0q}^h is a constant, which plays the role of the *thermodynamical potential* of the quark q^h and $\bar{x}$ is the *universal temperature*, which is the same for all partons. We recall that from the chiral structure of QCD, we have two important properties, allowing to relate quark and antiquark distributions and to restrict the gluon distribution [4, 5, 6]:

   - The potential of a quark q^h of helicity h is opposite to the potential of the corresponding antiquark $\bar{q}^{-h}$ of helicity $-h$

$$X_{0q}^h = -X_{0\bar{q}}^{-h} \ . \tag{2}$$

   - The potential of the gluon G is zero

$$X_{0G} = 0 \ . \tag{3}$$

Therefore similarly to Eq. (1), we have for the light antiquarks

$$x\bar{q}^h(x, Q_0^2) = \frac{\bar{A}(X_{0q}^{-h})^{-1} x^{2b}}{\exp[(x + X_{0q}^{-h})/\bar{x}] + 1} + \frac{\tilde{A}x^{\tilde{b}}}{\exp(x/\bar{x}) + 1} \ . \tag{4}$$

Here we take $2b$ for the power of x and not b as for quarks, an assumption which was discussed and partly justified in Ref. [1].
Concerning the unpolarized gluon distribution, we use a quasi Bose-Einstein function, with zero potential

$$xG(x, Q_0^2) = \frac{A_G x^{b_G}}{\exp(x/\bar{x}) - 1} \ . \tag{5}$$

This choice is consistent with the idea that hadrons, in the DIS regime, are black body cavities for the color fields. It is also reasonable to assume that for very small x, $xG(x, Q_0^2)$ has the same behavior as the diffractive contribution of the quark and antiquark distributions in Eqs. (1) and (4), so we will take $b_G = 1 + \tilde{b}$. We also need to specify the polarized gluon distribution and we take

$$x\Delta G(x, Q_0^2) = 0 \ , \tag{6}$$

assuming a zero polarized gluon distribution at the input energy scale Q_0^2. For the strange quarks and antiquarks, s and $\bar{s}$, given our poor knowledge on their unpolarized and polarized distributions, we take [2]

$$xs(x, Q_0^2) = x\bar{s}(x, Q_0^2) = \frac{1}{4}[x\bar{u}(x, Q_0^2) + x\bar{d}(x, Q_0^2)] \ , \tag{7}$$

and

$$x\Delta s(x, Q_0^2) = x\Delta\bar{s}(x, Q_0^2) = \frac{1}{3}[x\Delta\bar{d}(x, Q_0^2) - x\Delta\bar{u}(x, Q_0^2)] \ . \tag{8}$$

This particular choice gives rise to a large negative $\Delta s(x, Q_0^2)$. Both unpolarized and polarized distributions for the heavy quarks c, b, t, are set to zero at $Q_0^2 = 4 \text{GeV}^2$.

With the above assumptions, we note that the heavy quarks do not introduce any free parameters, likewise the gluons, since the normalization constant A_G in Eq. (5) is determined from the momentum sum rule. Among the parameters introduced so far in Eqs. (1) and (4), A and $\bar{A}$ are fixed by the two conditions $u - \bar{u} = 2$, $d - \bar{d} = 1$. Clearly these valence quark conditions are independent of $\tilde{b}$ and $\tilde{A}$, since the diffractive contribution cancels out. Therefore the light quarks require only *eight* free parameters, the *four* potentials X_{0u}^+, X_{0u}^-, X_{0d}^+, X_{0d}^-, *one* universal temperature $\bar{x}$, b, $\tilde{b}$ and $\tilde{A}$.

From well established features of the u and d quark distributions extracted from DIS data, we anticipate some simple relations between the potentials:
- $u(x)$ dominates over $d(x)$, therefore one expects $X_{0u}^+ + X_{0u}^- > X_{0d}^+ + X_{0d}^-$
- $\Delta u(x) > 0$, therefore $X_{0u}^+ > X_{0u}^-$
- $\Delta d(x) < 0$, therefore $X_{0d}^- > X_{0d}^+$.

So X_{0u}^+ should be the largest thermodynamical potential and X_{0d}^+ the smallest one. In fact, as we will see below, we have the following ordering

$$X_{0u}^+ > X_{0d}^- \sim X_{0u}^- > X_{0d}^+ \ . \tag{9}$$

---

[2] A strangeness asymmetry, $s(x) \neq \bar{s}(x)$, can be also obtained in the statistical approach [7]

This ordering leads immediately to some important consequences for quarks and antiquarks.

First, the fact that $X_{0d}^- \sim X_{0u}^-$, indicated in Eq. (9), leads to

$$u^-(x, Q_0^2) \lesssim d^-(x, Q_0^2) \ , \tag{10}$$

which implies from our procedure to construct antiquark from quark distributions,

$$\bar{u}^+(x, Q_0^2) \gtrsim \bar{d}^+(x, Q_0^2) \ . \tag{11}$$

These two important approximate relations were already obtained in Ref. [1], by observing in the data, the similarity in shape of the isovector structure functions $2xg_1^{(p-n)}(x)$ and $F_2^{(p-n)}(x)$, at the initial energy scale, as illustrated in Fig. 1 [3]. For $2xg_1^{(p-n)}(x)$ the black circles are obtained by combining SLAC [11] and JLab [12] data. The white circles, which extend down to the very low x region, include the recent deuteron data from COMPASS [13] combined with the proton data from SMC [10], at the measured Q^2 values of these two experiments [4]. The agreement with the curve of the statistical model is improved in this later case. The + helicity components disappear in the difference $2xg_1^{(p-n)}(x) - F_2^{(p-n)}(x)$. Since this difference is mainly non-zero for $0.01 < x < 0.3$, it is due to the contributions of $\bar{u}^-$ and $\bar{d}^-$ (see Ref. [1]).

Second, the ordering in Eq. (9) implies the following properties for antiquarks, namely:

i) $\bar{d}(x) > \bar{u}(x)$, the flavor symmetry breaking which also follows from the Pauli exclusion principle, as recalled above. This was already confirmed by the violation of the Gottfried sum rule [8, 9].

ii) $\Delta\bar{u}(x) > 0$ and $\Delta\bar{d}(x) < 0$, which have not been established yet, given the lack of precision of the polarized semi-inclusive DIS data, as we will see below. One expects an accurate determination of these distributions from the measurement of helicity asymmetries for weak boson production in polarized pp collisions at RHIC-BNL [14], which will allow this flavor separation.

By performing a next-to-leading order QCD evolution of these parton distributions, we were able to obtain in Ref. [1], a good description of a large set of very precise data on the following unpolarized and polarized DIS

---

[3]Notice that it differs from Fig. 1 in Ref. [1], where we put incorrect scales, both on the vertical and the horizontal axes

[4]We have not included some corrections due to difference of the beam energies of COMPASS and SMC
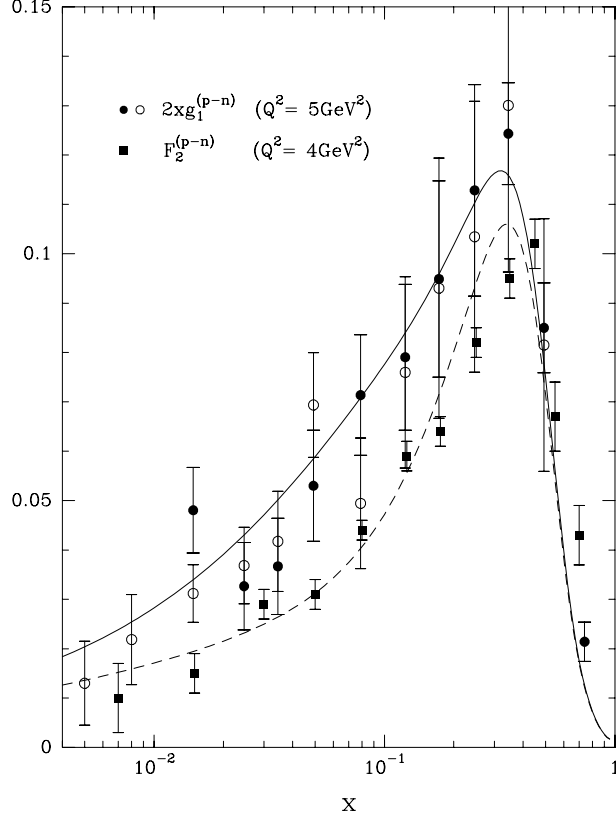
Figure 1: The isovector structure functions $2xg_1^{(p-n)}(x)$ (solid line from our statistical parton distributions) and $F_2^{(p-n)}(x)$ (dashed line from our statistical distributions). Data are from NMC [9], SMC [10], SLAC [11], JLab [12] and COMPASS [13].

structure functions $F_2^{p,d,n}(x, Q^2), xF_3^{\nu N}(x, Q^2)$ and $g_1^{p,d,n}(x, Q^2)$, in a broad range of x and Q^2, in correspondance with the *eight* free parameters :

$$X_{0u}^+ = 0.46128, \ X_{0u}^- = 0.29766, \ X_{0d}^- = 0.30174, \ X_{0d}^+ = 0.22775 , \qquad (12)$$

$$\bar{x} = 0.09907, \ b = 0.40962, \ \tilde{b} = -0.25347, \ \tilde{A} = 0.08318 , \qquad (13)$$

and three additional parameters, which are fixed by normalization conditions

$$A = 1.74938, \ \bar{A} = 1.90801, \ A_G = 14.27535 , \qquad (14)$$

as explained above. Note that the numerical values of the four potentials are in agreement with the ordering in Eq. (9), as expected, and all the free parameters in Eqs. (12, 13) have been determined rather precisely, with an error of the order of one percent.

3   The predicting power of the statistical parton distributions

We now try to relate the x dependence of the quark (antiquark) distributions to their specific expressions given in Eqs. (1) and (4) and to study the role of the different free parameters involved, according to their numerical values obtained in Ref. [1]. First, it is useful to note that, given the small value of $\tilde{A}$ (see Eq. (13)), the diffractive contribution is less than 10^{-2} or so, for $x \geq 0.1$, but it dominates in the very low x region, when $x << \bar{x}$, since $\tilde{b} < 0$. Therefore the strong change of slope of $xu(x)$ and $xd(x)$ at high x (at the input scale Q_0^2 and above), is related to the values of the corresponding potentials and is larger for u than for d, because of the ordering in Eq. (9). This is indeed what we observe in Fig. 2, at some rather high Q^2 values. This feature is not spoilt by the Q^2 evolution, which is also well described by the statistical quark distributions as shown in Fig. 3, where we compare with H1 data. Another interesting point concerns the behavior of the ratio $d(x)/u(x)$, which depends on the mathematical properties of the ratio of two Fermi-Dirac factors, outside the region dominated by the diffractive contribution. So for $x > 0.1$, this ratio is expected to decrease faster for $X_{0d}^+ - \bar{x} < x < X_{0u}^+ + \bar{x}$ and then above, for $x > 0.6$ it flattens out. This change of slope is clearly visible in Fig. 4, with a very little Q^2 dependence. Note that our prediction for the large x behavior, differs from most of the current literature, namely $d(x)/u(x) \to 0$ for $x \to 1$, but we find $d(x)/u(x) \to 0.16$ near the value $1/5$, a prediction originally formulated in Ref. [16]. This is a very challenging question, since the very high x region remains poorly known, as shown in Fig. 2 and Fig. 3. The typical behaviour of the Fermi-Dirac functions, falling down exponentially above the thermodynamical potential, which shows up in Fig. 1, complies well with the fast change in the slope of $g_1^p(x)$ at high x, as shown in Fig. 6.

Analogous considerations can be made for the corresponding helicity distributions, whose best determinations are shown in Fig. 5. By using a sim-

ilar argument as above, the ratio $\Delta u(x)/u(x)$ is predicted to have a rather fast increase in the x range $(X_{0u}^- - \bar{x}, X_{0u}^+ + \bar{x})$ and a smoother behaviour above, while $\Delta d(x)/d(x)$, which is negative, has a fast decrease in the x range $(X_{0d}^+ - \bar{x}, X_{0d}^- + \bar{x})$ and a smooth one above. This is exactly the trends displayed in Fig. 5 and our predictions are in perfect agreement with the accurate high x data [5]. We note the behavior near $x = 1$, another typical property of the statistical approach, also at variance with predictions of the current literature. The fact that $\Delta u(x)$ is more concentrated in the higher x region than $\Delta d(x)$, accounts for the change of sign of $g_1^n(x)$, which becomes positive for $x > 0.5$, as first observed at Jefferson Lab [12].

For the light antiquark distributions (see Eq. (4)), it is clear that in the very low x region $(x < 10^{-3})$ the ratio $\bar{d}(x)/\bar{u}(x)$ is ~ 1, since the diffractive contribution dominates [6] and it is an increasing function of x because the non diffractive term is larger for $\bar{d}(x)$ than for $\bar{u}(x)$. This natural expectation, $\bar{d}(x) \geq \bar{u}(x)$ from the statistical approach, was already mentioned above and has been also confirmed by the E866/NuSea Drell-Yan dilepton experiment [20], up to $x = 0.15$. For larger x, although the errors are large, the data seem to drop off in disagreement with our predictions (see Fig. 16 in Ref. [1]). This important point deserves further attention and we will come back to it in Section 6, when we will discuss Drell-Yan dilepton cross sections. This is another challenging point, which needs to be clarified, for example with future measurements by the approved FNAL E906 experiment [21], to higher x values.

We now turn to the antiquark helicity distributions. Since we predict $\Delta \bar{u}(x) > 0$ and $\Delta \bar{d}(x) < 0$, the contribution of the antiquarks to the Bjorken sum rule (BSR) [22] is in our case 0.022, at $Q^2 = 5\text{GeV}^2$, which is not negligible. The statistical model gives for the BSR the value 0.176, in excellent agreement with the QCD prediction 0.182 ± 0.005 and with the world data $0.176 \pm 0.003 \pm 0.07$ [11]. It is also interesting to remark that Eq. (11) implies

$$\Delta \bar{u}(x) - \Delta \bar{d}(x) \simeq \bar{d}(x) - \bar{u}(x) > 0 \ , \tag{15}$$

so the flavor asymmetry of the light antiquark distributions is almost the same for the corresponding helicity distributions. Similarly, Eq. (10) implies

---

[5]It is worth mentioning that the Jefferson Lab points for the d quark are those of Ref. [18], which have been moved down compared to those of Ref. [12]

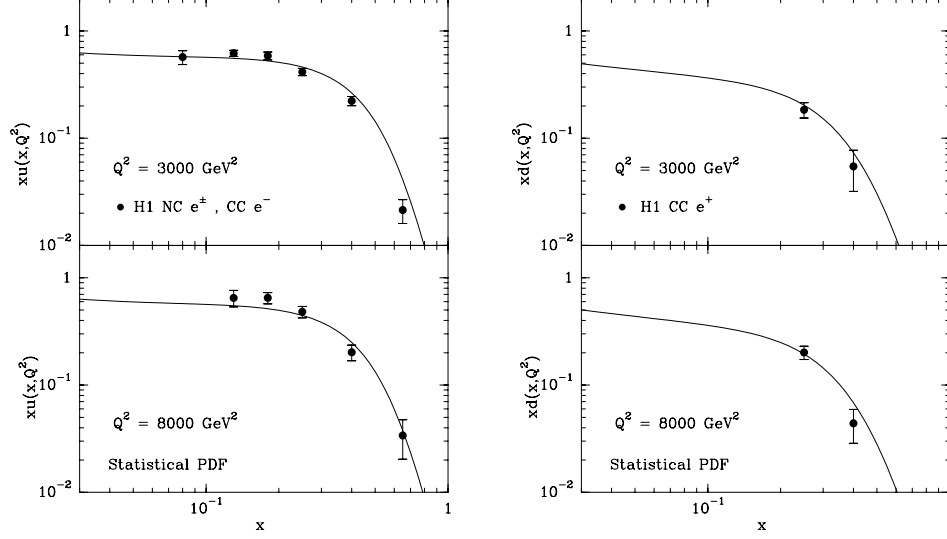[6]Obviously, this is also the case for the ratio $d(x)/u(x)$

Figure 2: Statistical quark distributions $xu(x, Q^2)$, $xd(x, Q^2)$ as a function of x for $Q^2 = 3000, 8000 \text{GeV}^2$. Data from H1 [15].

$$\Delta u(x) - \Delta d(x) \simeq u(x) - d(x) > 0 \ . \qquad (16)$$

By combining Eqs. (15) and (16), we find a very simple approximate result for the BSR, namely $\sim 1/6$, a value compatible with the numbers quoted above. We also compare in Fig. 7 our predictions with an attempt from Hermes to isolate the different quark and antiquark helicity distributions. The poor quality of the data does not allow to conclude on the signs of $\Delta \bar{u}(x)$ and $\Delta \bar{d}(x)$, which will have to wait for a higher precision experiment.

Finally we are coming back to the polarized gluon distribution $\Delta G(x, Q^2)$, which was assumed to be zero at the input scale $Q_0^2 = 4 \text{GeV}^2$ (see Eq. (6)). It is interesting to note that after evolution, it becomes negative for $Q^2 < Q_0^2$ and positive for $Q^2 > Q_0^2$. The results are displayed in Fig. 8 and are waiting for an improved experimental determination of this important distribution.

Figure 3: Statistical quark distributions $c \cdot xu(x, Q^2)$, $c \cdot xd(x, Q^2)$ as a function of Q^2 for fixed x bins. Data from H1 [15].
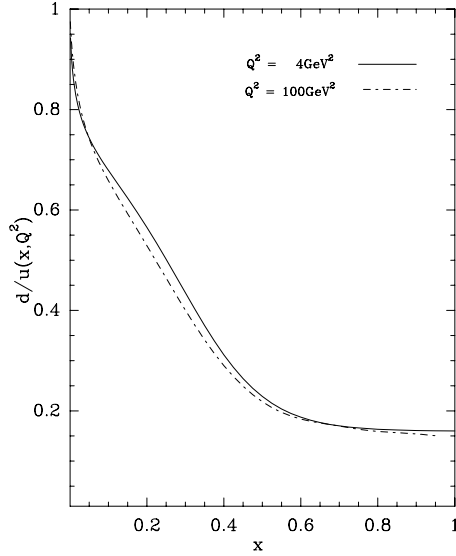

Figure 4: The quarks ratio d/u as function of x for $Q^2 = 4\mathrm{GeV}^2$ (solid line) and $Q^2 = 100\mathrm{GeV}^2$ (dashed-dotted line).
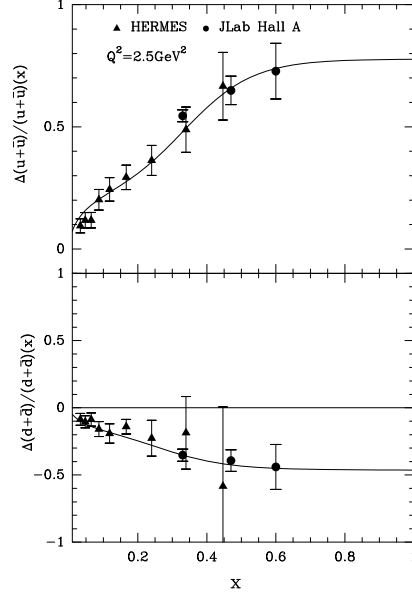
Figure 5: Ratios $(\Delta u + \Delta \bar{u})/(u + \bar{u})$ and $(\Delta d + \Delta \bar{d})/(d + \bar{d})$ as a function of x. Data from Hermes for $Q^2 = 2.5 \text{GeV}^2$ [17] and a JLab experiment [18]. The curves are predictions from the statistical approach.

Figure 6: $g_1^p(x, Q^2)$ as a function of x at fixed $Q^2 = 3\text{GeV}^2$ from the statistical approach. Experimental data from SLAC E143 [19].

Figure 7: Quarks and antiquarks polarized parton distributions as a function of x for $Q^2 = 2.5\text{GeV}^2$. Data from Hermes [23]. The curves are predictions from the statistical approach.
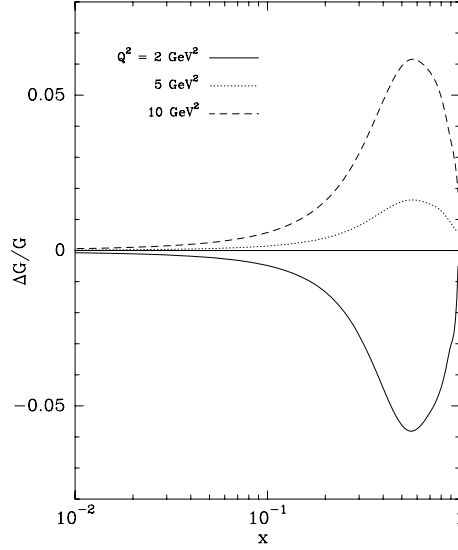

Figure 8: The ratio $\Delta G(x)/G(x)$ as a function of x, for $Q^2 = 2, 5$ and $10\ \text{GeV}^2$. The curves are predictions from the statistical approach.

12

4 Inclusive neutral and charged current $e^{\pm}p$ cross sections

The neutral current DIS processes have been measured at HERA in a kinematic region where both the γ and the Z exchanges must be considered. The cross sections for neutral current can be written, at lowest order, as [24]

$$\frac{d^2\sigma_{NC}^{\pm}}{dxdQ^2} = \frac{2\pi\alpha^2}{xQ^4}\left[Y_+\tilde{F}_2(x,Q^2) \mp Y_-x\tilde{F}_3(x,Q^2) - y^2\tilde{F}_L(x,Q^2)\right] ,\qquad (17)$$

where

$$\tilde{F}_2(x,Q^2) = F_2^{em} - v_e\chi_z(Q^2)G_2(x,Q^2) + (a_e^2+v_e^2)\chi_z^2(Q^2)H_2(x,Q^2) ,\quad (18)$$

$$x\tilde{F}_3(x,Q^2) = -a_e\chi_z(Q^2)xG_3(x,Q^2) + 2a_ev_e\chi_z^2(Q^2)xH_3(x,Q^2) .\qquad (19)$$

The structure function $\tilde{F}_L(x,Q^2)$ is sizeable only at high y and the other structure functions introduced above, have the following expressions in terms of the parton distributions

$$[F_2^{em}, G_2, H_2](x,Q^2) = \sum_f \left[Q_f^2, 2Q_f v_f, a_f^2+v_f^2\right]\left(xq_f(x,Q^2)+x\bar{q}_f(x,Q^2)\right),$$

$$[xG_3, xH_3](x,Q^2) = \sum_f \left[2Q_f a_f, 2a_f v_f\right]\left(xq_f(x,Q^2)-x\bar{q}_f(x,Q^2)\right).\quad (20)$$

Here the kinematic variables are $y = Q^2/xs$, $Y_{\pm} = 1\pm(1-y)^2$, $\sqrt{s} = \sqrt{E_eE_p}$, E_e and E_p are the electron (positron) and proton beam energies respectively. Morever, v_i and a_i are the vector and axial-vector weak coupling constants for the lepton e and the quark f, respectively, and Q_f is the charge. The function $\chi_z(Q^2)$ is given by

$$\chi_z(Q^2) = \frac{1}{4\sin^2\theta_W\cos^2\theta_W}\frac{Q^2}{Q^2+M_Z^2} ,\qquad (21)$$

where θ_W is the weak mixing angle and M_Z is the Z-boson mass. The reduced cross sections are defined as

$$\tilde{\sigma}_{NC}^{\pm}(x,Q^2) = \frac{Q^4x}{Y_+2\pi\alpha^2}\frac{d^2\sigma_{NC}^{\pm}}{dxdQ^2} .\qquad (22)$$

Our predictions are compared with H1 and ZEUS data in Figs. 9 and 10, as a function of x, in a broad range of Q^2 values and the agreement is excellent.

The charged current DIS processes have been also measured accurately at HERA in an extented kinematic region. It has a serious impact on the determination of the unpolarized parton distributions by allowing a flavor separation because they involve only the $W^\pm$ exchange. The cross sections are expressed, at lowest order, in terms of three structure functions as follows [24]

$$
\begin{aligned}
\frac{d^2\sigma_{Born}^{cc}}{dxdQ^2} \;=\; & \frac{G_F^2}{4\pi}\frac{M_W^4}{(Q^2+M_W^2)^2}\left[Y_+ F_2^{cc}(x,Q^2) - y^2 F_L^{cc}(x,Q^2)\right. \\
& \left. + Y_- x F_3^{cc}(x,Q^2)\right]\;,
\end{aligned}
\tag{23}
$$

and the reduced cross sections are defined as

$$
\tilde{\sigma}^{cc}(x,Q^2) = \left[\frac{G_F^2}{4\pi}\frac{M_W^4}{(Q^2+M_W^2)^2}\right]^{-1}\frac{d^2\sigma^{cc}}{dxdQ^2}\;.
\tag{24}
$$

At leading order for $e^- p \to \nu_e X$ with a longitudinally polarized beam

$$
\begin{aligned}
F_2^{cc}(x,Q^2) \;&=\; x[u(x,Q^2) + c(x,Q^2) + \bar{d}(x,Q^2) + \bar{s}(x,Q^2)] \\
x F_3^{cc}(x,Q^2) \;&=\; x[u(x,Q^2) + c(x,Q^2) - \bar{d}(x,Q^2) - \bar{s}(x,Q^2)]\;,
\end{aligned}
\tag{25}
$$

and for $e^+ p \to \bar{\nu}_e X$

$$
\begin{aligned}
F_2^{cc}(x,Q^2) \;&=\; x[d(x,Q^2) + s(x,Q^2) + \bar{u}(x,Q^2) + \bar{c}(x,Q^2)] \\
x F_3^{cc}(x,Q^2) \;&=\; x[d(x,Q^2) + s(x,Q^2) - \bar{u}(x,Q^2) - \bar{c}(x,Q^2)]\;.
\end{aligned}
\tag{26}
$$

At NLO in QCD F_L^{cc} is non zero, but it gives negligible contribution, except at y values close to 1. Our predictions are compared with H1 and ZEUS data in Figs. 11, 12, 13 and 14, as a function of x in a broad range of Q^2 values and vice versa. The agreement is very good, but unfortunately since the highest x value is only 0.42, it does not allow to clarify the situation regarding the large x behavior, as already noticed above.
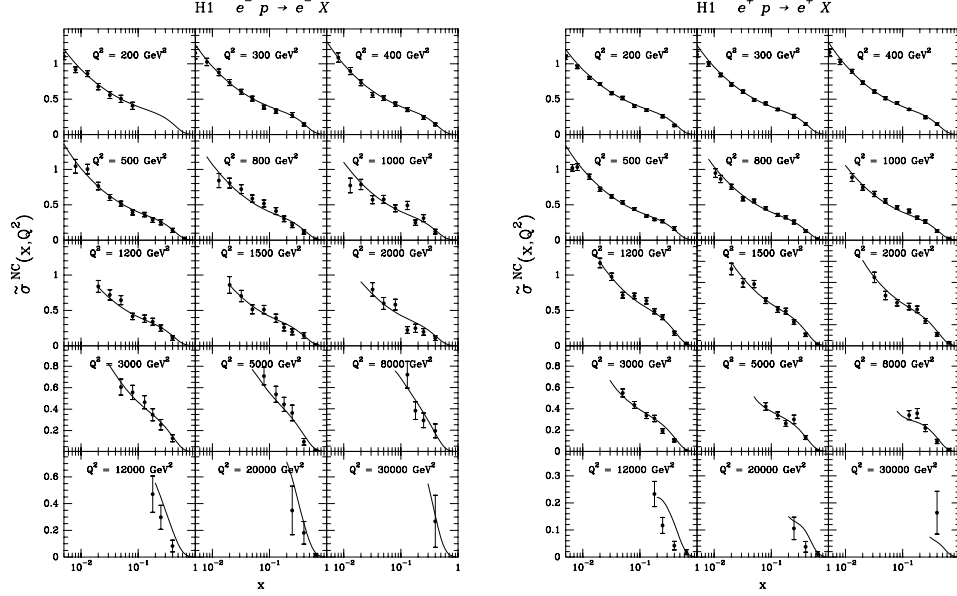
14

Figure 9: The reduced neutral current cross section $\tilde{\sigma}$, as a function of x, for different fixed values of Q^2. Reaction $e^- p$ at $\sqrt{s} = 320\text{GeV}$, $e^+ p$ at $\sqrt{s} = 319\text{GeV}$. Data from H1 [15, 25]. The curves are predictions from the statistical approach.
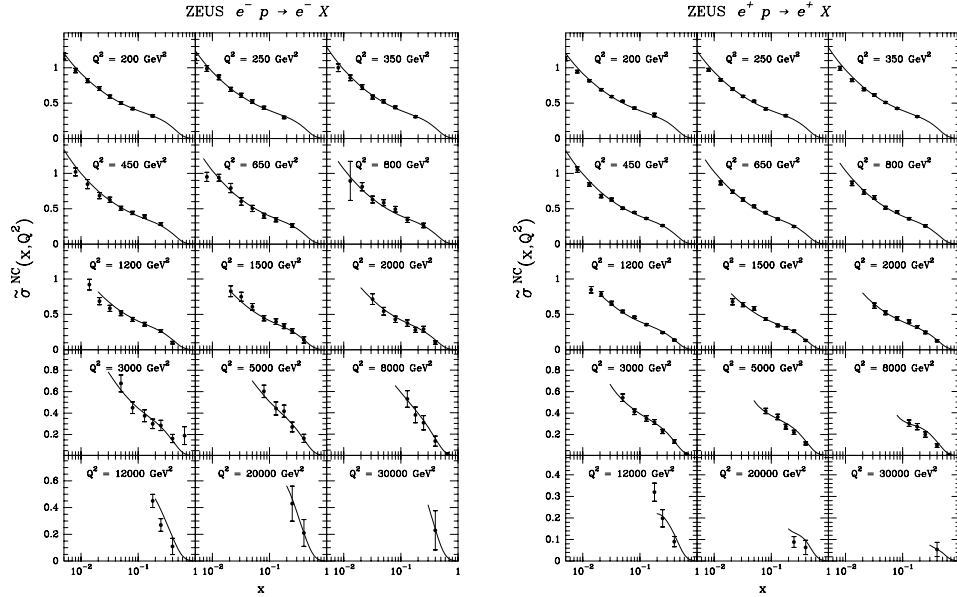

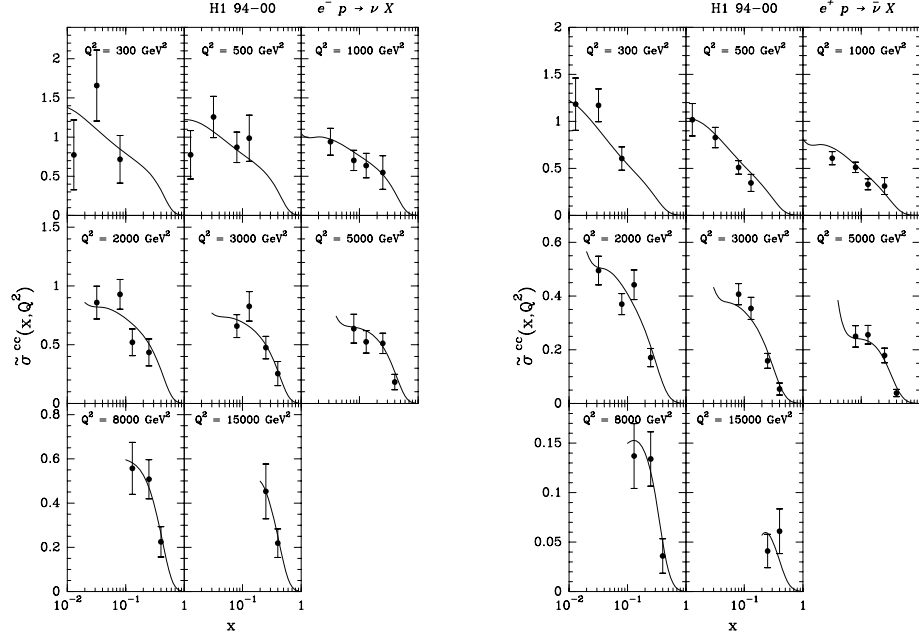Figure 10: Same as Fig. 9. Data from ZEUS [26].

15

Figure 11: The reduced charged current cross section $\tilde{\sigma}$, in $e^{\pm}p$ reactions as a function of x, for different fixed values of Q^2. Data from H1 [15, 25].

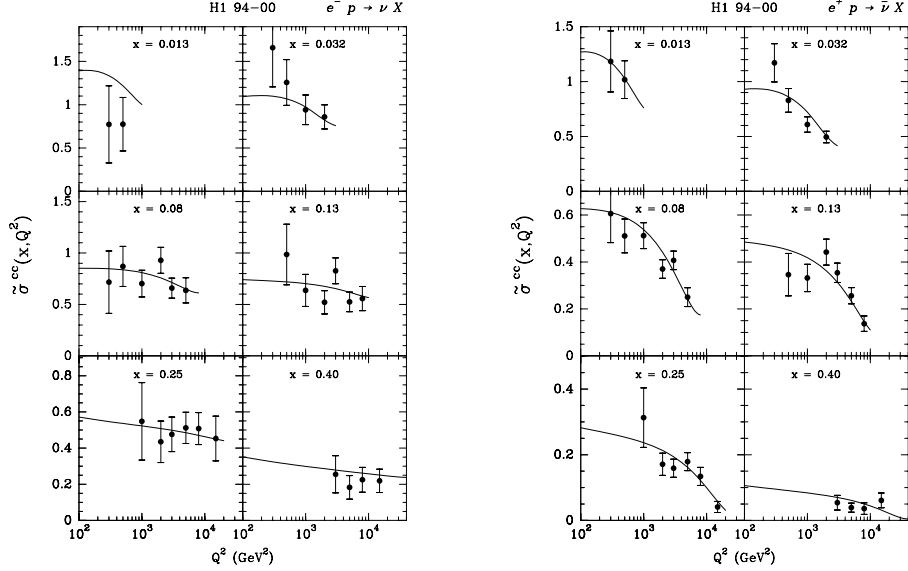

Figure 12: The reduced charged current cross section $\tilde{\sigma}$, in $e^{\pm}p$ reactions as a function of Q^2, for different fixed values of x. Data from H1 [15, 25].
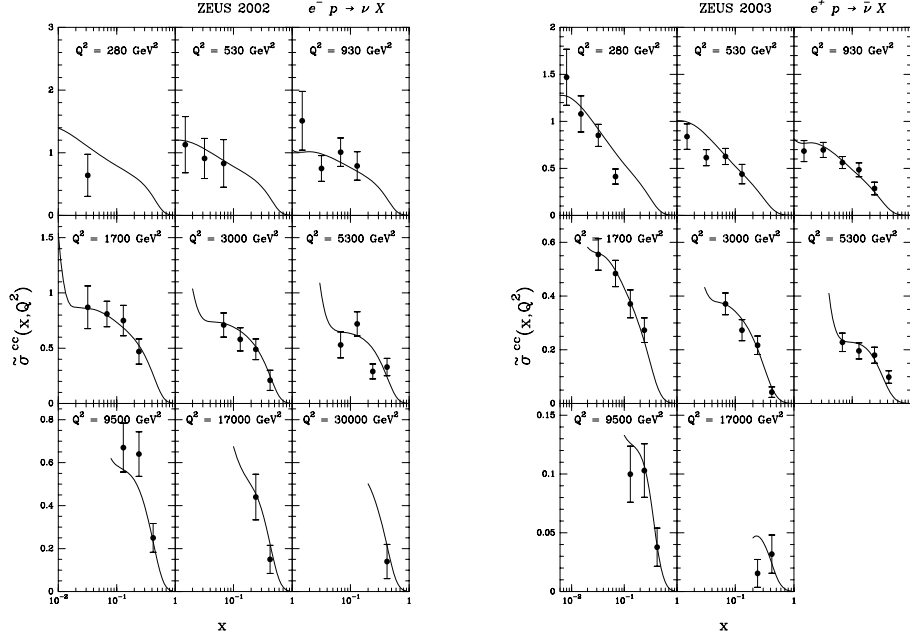
16

Figure 13: The reduced charged current cross section, $\tilde{\sigma}$, in $e^{\pm}p$ reactions as a function of x, for different fixed values of Q^2. Data from ZEUS [26, 27].
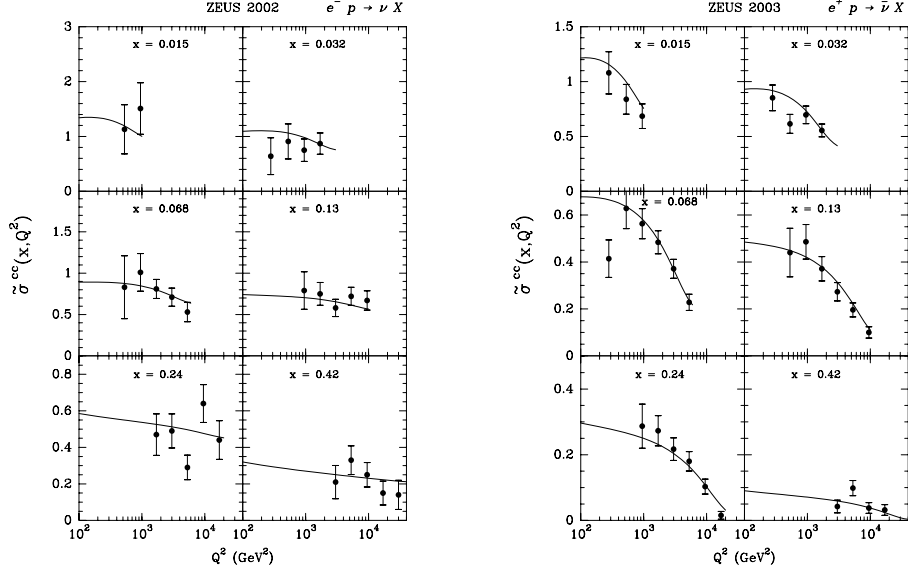

Figure 14: The reduced charged current cross section $\tilde{\sigma}$, in $e^{\pm}p$ reactions as a function of Q^2, for different fixed values of x. Data from ZEUS [26, 27].

17

5   Charged current neutrino cross sections

The differential inclusive neutrino and antineutrino cross sections have the following standard expressions

$$
\begin{aligned}
\frac{d^2\sigma^{\nu,(\bar{\nu})}}{dxdy} &= \frac{G_F^2 M_p E_\nu}{\pi(1+\frac{Q^2}{M_W^2})^2}\left[xy^2 F_1^{\nu(\bar{\nu})}(x,Q^2) + (1-y-\frac{M_p xy}{2E_\nu})F_2^{\nu(\bar{\nu})}(x,Q^2)\right. \\
&\left. \pm(y-\frac{y^2}{2})xF_3^{\nu(\bar{\nu})}(x,Q^2)\right],
\end{aligned}
\tag{27}
$$

y is the fraction of total leptonic energy transfered to the hadronic system and E_ν is the incident neutrino energy. F_2 and F_3 are given by Eq. (25) for νp and Eq. (26) for $\bar{\nu}p$, and F_1 is related to F_2 by

$$
2xF_1 = \frac{1+4M_p^2 x^2}{1+R}F_2,
\tag{28}
$$

where $R = \sigma_L/\sigma_T$, the ratio of the longitudinal to transverse cross sections of the W-boson production. The calculations are done with $\sin^2\theta_W = 0.2277\pm0.0013\pm0.009$ obtained by NuTeV [28] and the comparison with the CCFR and NuTeV data are shown in Fig. 15. As expected, for fixed x, the y dependence is rather flat for neutrino and has the characteristic $(1-y)^2$ behavior for antineutrino.

This can be extrapolated to evaluate the cross section of ultrahigh energy neutrinos with nucleons. The total cross section at a given neutrino energy reads

$$
\sigma_{\nu N}^{CC}(E_\nu) = \int dxdy\frac{d^2\sigma^{\nu,(\bar{\nu})}}{dxdy}.
\tag{29}
$$

Our prediction for this total charged current cross section, for an isoscalar nucleon $N = 1/2(p+n)$, versus the neutrino energy, is displayed in Fig. 16 and it has the expected strong energy increase. We have not calculated the corresponding neutral current cross section, which is known to be a factor three or so smaller. This new information is certainly valuable to the large scale neutrino telescopes, for the detection of extraterrestrial neutrino sources.
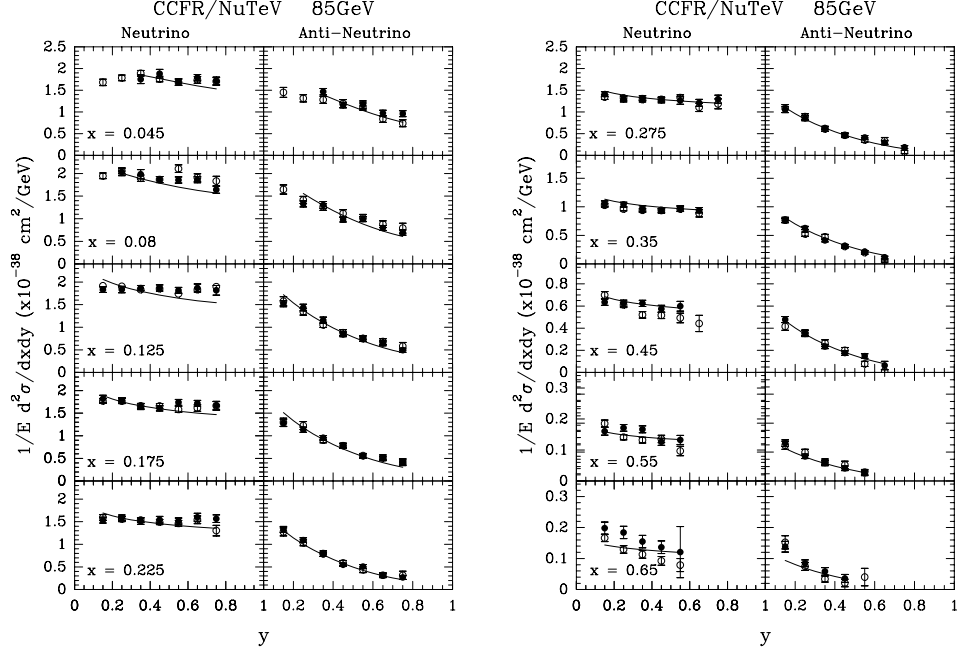
Figure 15: Differential cross section $\nu(\bar{\nu})N$ for $E_\nu = 85\text{GeV}$, as a function of y. Data are from CCFR [29] (white circles) and NuTeV experiments [30, 31] (black circles).
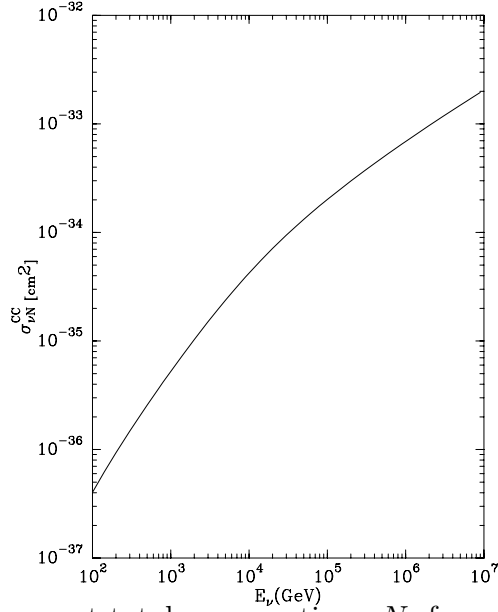

Figure 16: Charged current total cross section νN, for an isoscalar target as a function of the neutrino energy.

19

6 Drell-Yan dilepton cross sections

A very important source of information for $\bar{q}(x)$ distributions comes from Drell-Yan dilepton processes, whose cross sections are proportional to a combination of products of $q(x)$ and $\bar{q}(x)$ distributions. The cross section $\sigma_{DY}(pp)$ for $pp \to \mu^+ \mu^- X$, at the lowest order, has the simplified form

$$M^3 \frac{d^2\sigma_{DY}(pp)}{dMdx_F} = \frac{8\pi\alpha^2}{9(x_1 + x_2)} \sum_i e_i^2 [q_i(x_1)\bar{q}_i(x_2) + \bar{q}_i(x_1)q_i(x_2)] , \qquad (30)$$

where M is the invariant mass of the produced muon pair, x_1 and x_2 refer to the beam and target respectively, $x_F = x_1 - x_2$ and $M^2 = x_1 x_2 s$, where $\sqrt{s}$ is the center of mass energy of the collision. Clearly at NLO one should add the Compton processes contributions to the above $q\bar{q}$ annihilation terms.

More recently the NuSea Collaboration has released the data on the Drell-Yan cross sections $\sigma_{DY}(pp)$ and $\sigma_{DY}(pd)$ for proton-proton and proton-deuterium collisions at 800 GeV/c [32]. They are displayed in Fig. 17 as a function of x_F for selected M bins, together with our predictions. The agreement is fairly good, mainly in the small mass region, but in order to evaluate it more precisely, we have plot in Fig. 18 the ratios of experiment versus theory, using a broader set of data.

Let us now come back to the extraction of the ratio $\bar{d}/\bar{u}$ from these data. For large x_F, namely $x_1 >> x_2$ and small M, we have

$$\frac{\sigma_{DY}(pd)}{2\sigma_{DY}(pp)} \simeq 1/2 \left[1 + \frac{\bar{d}(x_2)}{\bar{u}(x_2)} \right] , \qquad (31)$$

so the measurement of this cross sections ratio is directly related to $\bar{d}(x)/\bar{u}(x)$ for small x. For large x one needs to use small x_F and large M values and we have now for $x_1 \simeq x_2$

$$\frac{\sigma_{DY}(pd)}{2\sigma_{DY}(pp)} \simeq 1/2 \left[\frac{8 + 5\frac{\bar{d}(x)}{\bar{u}(x)} + 5\frac{d(x)}{u(x)} + 2\frac{\bar{d}(x)}{\bar{u}(x)}\frac{d(x)}{u(x)}}{8 + 2\frac{\bar{d}(x)}{\bar{u}(x)}\frac{d(x)}{u(x)}} \right] . \qquad (32)$$

Therefore the falloff at large x of $\sigma_{DY}(pd)/2\sigma_{DY}(pp)$ observed in Ref.[20] cannot be directly related to the falloff of $\bar{d}(x)/\bar{u}(x)$, since $d(x)/u(x)$ is also decreasing for large x, as shown previously (see Fig. 4). The use of Eq. (31) will lead to an underestimation of $\bar{d}(x)/\bar{u}(x)$. We also notice in Fig. 17 an experimental point for $\sigma_{DY}(pp)$ in the bin with M in the range (10.85,11.85)GeV
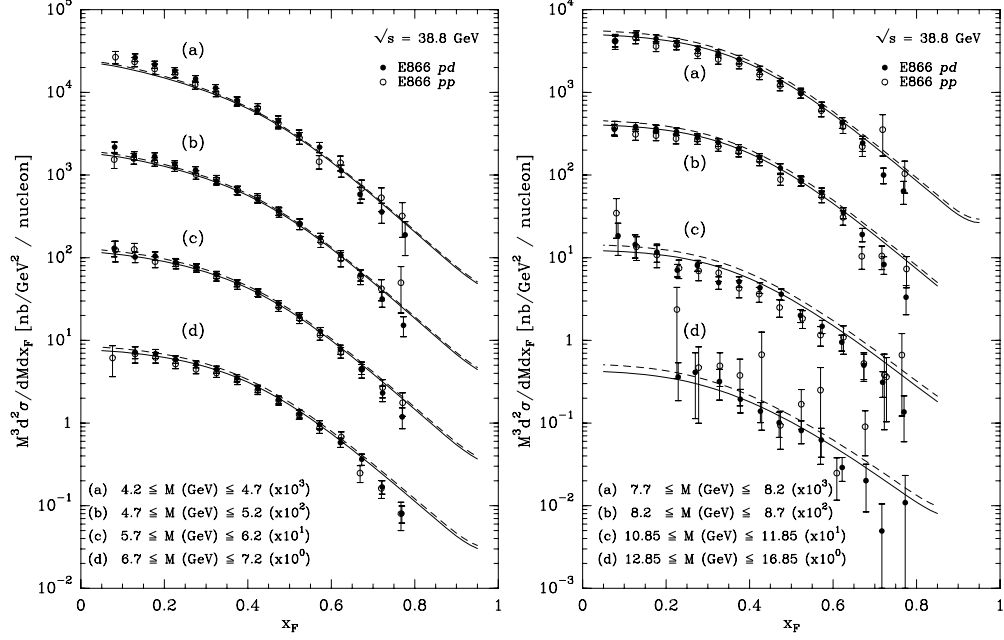
20

Figure 17: Drell-Yan cross sections per nucleon at $\sqrt{s} = 38.8$GeV for pp and pd as a function of x_F for selected M bins. Solid curve pp, dashed curve pd. Experimental data from FNAL E866 [32].

at $x_F \simeq 0.05$, two standard deviations above our curve, which might very well be one of the reason for the dramatic falling off of $\bar{d}(x)/\bar{u}(x)$ for $x \simeq 0.3$, reported by NuSea. Obviously more accurate data in this region are badly needed.
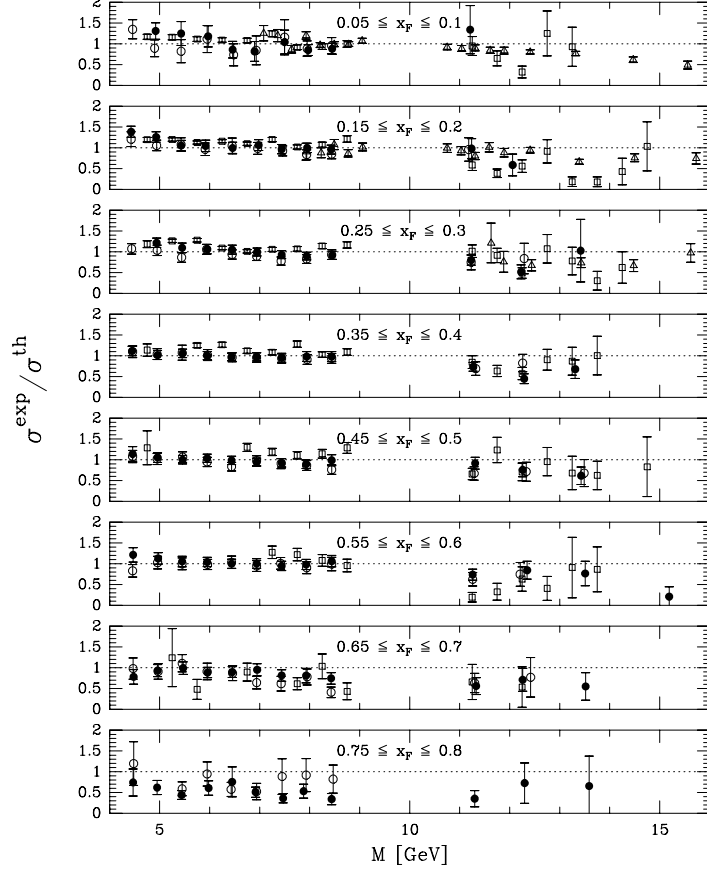
Figure 18: Drell-Yan cross sections ratios experiment versus theory at $\sqrt{s} = 38.8\text{GeV}$ for pp (open circle), pd (full circle, square), and pCu (triangle) as a function of M for selected x_F bins. Experimental data are from Refs. [32, 33, 34].

7 Single jet and π^0 inclusive productions

A precise determination of parton distributions allows us to use them as input information to predict strong interaction processes, for additional tests of pertubative QCD and also for the search of new physics. Here we shall test our statistical parton distributions for the description of two inclusive reactions, single jet and π^0 productions. The cross section for the production of a single jet of rapidity y and transverse momentum p_T, in a $\bar{p}p$ collision is given by

$$
\begin{aligned}
E\frac{d^3\sigma}{dp^3} &= \sum_{ij} \frac{1}{1+\delta_{ij}} \frac{2}{\pi} \int_{x_0}^1 dx_a \frac{x_a x_b}{2x_a - x_T e^y} \times \\
&\qquad \left[f_i(x_a, Q^2) f_j(x_b, Q^2) \frac{d\hat{\sigma}_{ij}}{d\hat{t}}(\hat{s}, \hat{t}, \hat{u}) + (i \leftrightarrow j) \right] ,
\end{aligned} \tag{33}
$$

where $x_T = 2p_T/\sqrt{s}$, $x_0 = x_T e^y/(2 - x_T e^{-y})$, $x_b = x_a x_T e^{-y}/(2x_a - x_T e^y)$ and $\sqrt{s}$ is the center of mass energy of the collision. In the above sum, i, j stand for initial gluon-gluon, quark-gluon and quark-quark scatterings, $d\hat{\sigma}_{ij}/d\hat{t}$ are the corresponding partonic cross sections and Q^2 is the scaling variable. The NLO QCD calculations at $\mathcal{O}(\alpha_s^3)$, were done using a code described in Ref. [35], based on a semi-analytical method within the "small-cone approximation"[7].

In Fig. 19 our results are compared with the data from CDF and D0 experiments [36, 37]. Our prediction agrees very well with the data up to the highest E_T (or p_T) value and this is remarkable given the fact that the experimental results are falling off over more than six orders of magnitude, leaving no room for new physics. For completeness, we also show in Fig. 20 the D0 data, for several rapidity bins, using a (Data-Theory)/Theory presentation.

Next we consider the cross section for the inclusive production of a π^0 of rapidity y and transverse momentum p_T, in a pp collision, which has the

---

[7]We thank Werner Vogelsang for providing us with the numerical values, resulting from the use of our parton distributions

following expression

$$
\begin{aligned}
E_\pi d^3\sigma/dp_\pi^3 &= \sum_{abc} \int dx_a dx_b \, f_{a/p}(x_a, Q^2) \times \\
&\qquad f_{b/p}(x_b, Q^2) \frac{D_{\pi^0/c}(z_c, Q^2)}{\pi z_c} d\hat\sigma/d\hat t (ab \to cX) \ , \qquad (34)
\end{aligned}
$$

where the sum is over all the contributing partonic channels $ab \to cX$ and $d\hat\sigma/d\hat t$ is the associated partonic cross section. In these calculations $f_{a/p}, f_{b/p}$ are our parton distributions and $D_{\pi^0/c}$ is the pion fragmentation function. Our calculations are done up to the NLO corrections, using the numerical code INCNLL of Ref. [39] and for two different choices of fragmentation functions namely, BKK of Ref. [40] and KKP of Ref. [41], and we have checked that they give similar numerical results. We have compared our predictions to two different data sets at $\sqrt{s} = 200\text{GeV}$ from PHENIX and STAR at RHIC-BNL. The results are shown in Figs. 21 and 22 and the agreement is good, both in central rapidity region (PHENIX) and in the forward region (STAR). This energy is high enough to expect NLO QCD calculations to be valid in a large rapidity region, which is not the case for lower energies [44].
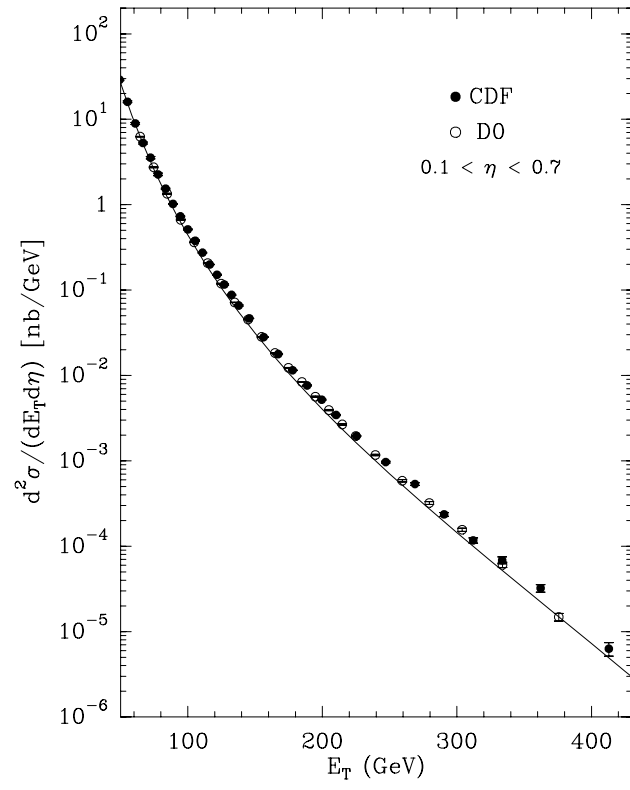
Figure 19: Cross section for single jet production in $\bar{p}p$ at $\sqrt{s} = 1.8\text{TeV}$ as a function of E_T. Data are from CDF [36] and D0 [37] experiments.
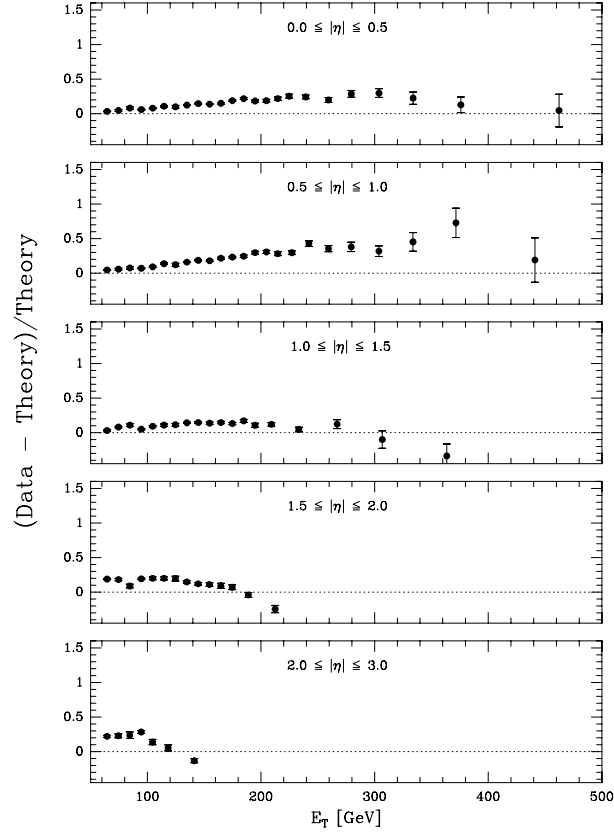
Figure 20: Comparison between the statistical model and the D0 [38] single jet cross sections in $\bar{p}p$ at $\sqrt{s} = 1.8\text{TeV}$, as a function of E_T and rapidity η.
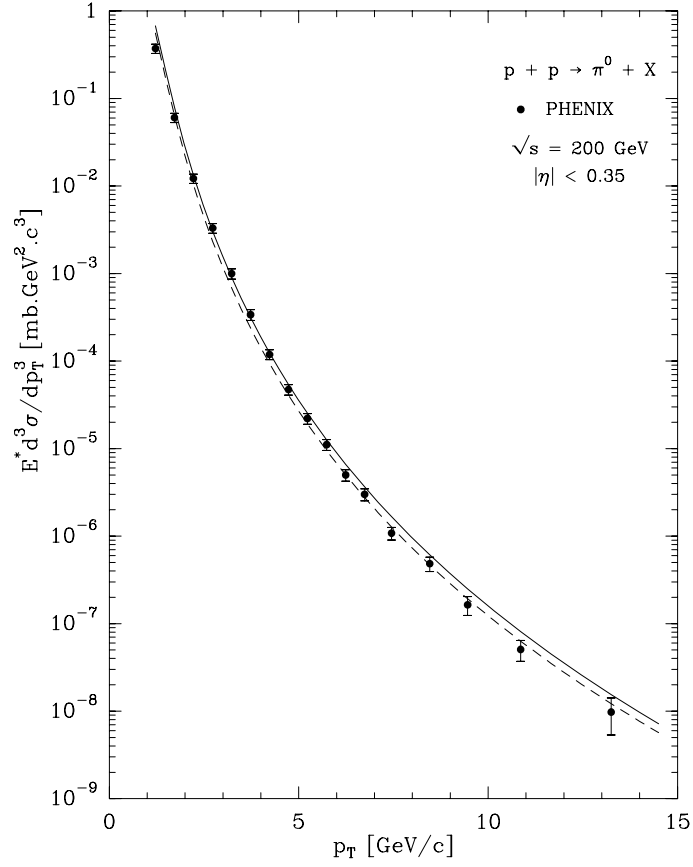
Figure 21: Inclusive π^0 production in pp reaction at $\sqrt{s} = 200\text{GeV}$ as a function of p_T, scale $\mu = p_T$. Data from PHENIX [42]. Solid curve fragmentation functions from KKP [41], dashed curve from BKP [40].
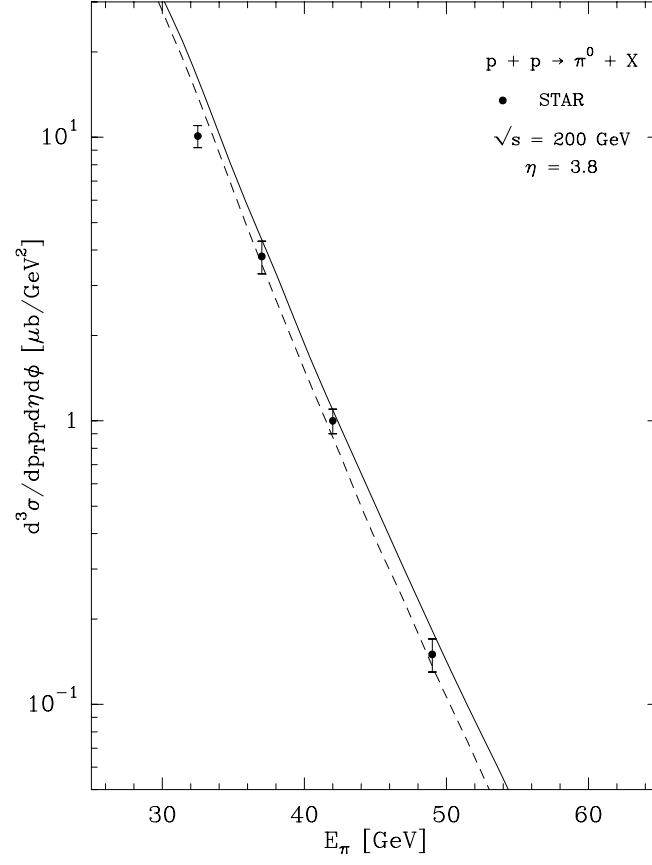
Figure 22: Inclusive π^0 production in pp reaction at $\sqrt{s} = 200$GeV as a function of E_π. Data from STAR [43]. Solid curve fragmentation functions from KKP [41], dashed curve from BKP [40].
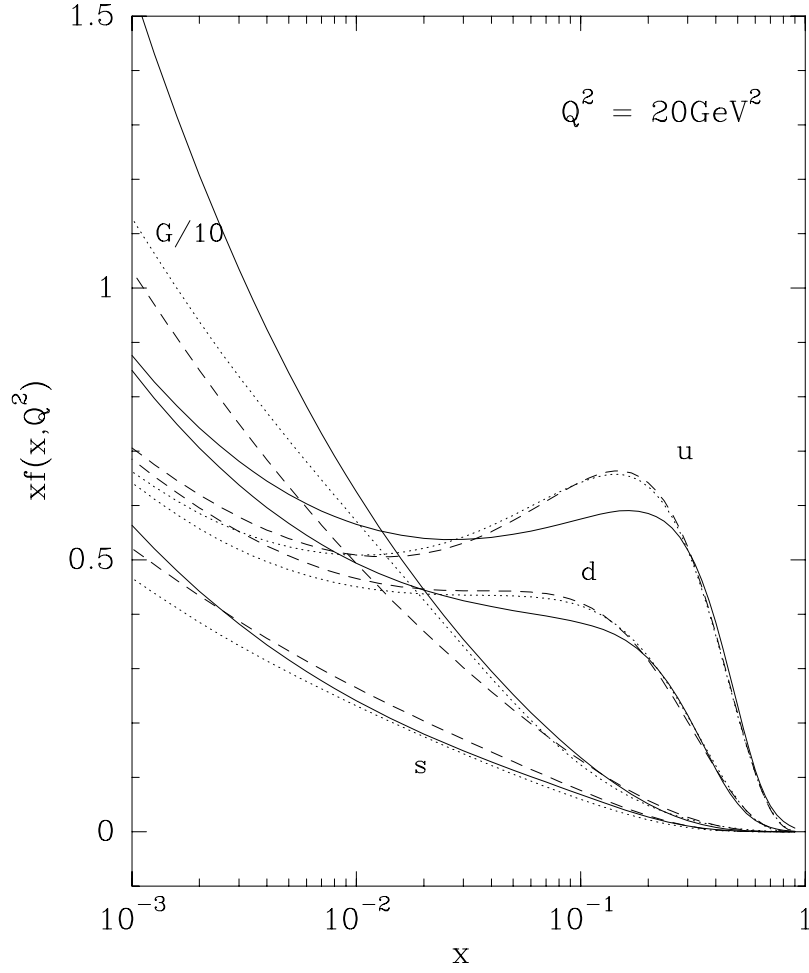
Figure 23: A comparison of the PDF at NLO from the statistical model (solid) with MRST2002 (dashed) [45] and CTEQ6 (dotted) [46], for quarks u, d, s and gluon at $Q^2 = 20\text{GeV}^2$.

29

8 Concluding remarks

We have shown that this simple approach of the statistical parton distributions provides a good description of recent data on unpolarized and polarized DIS and on several hadronic processes. Since it involves only eight free parameters, we have tried to relate them to some specific properties of the parton distributions, but we do not have yet a full understanding of their physical interpretation. It is important to stress that we have simultaneously the unpolarized and the polarized parton distributions, which is a unique situation. The main features of our distributions agree with other sets available in the literature, both in the unpolarized case [45, 46] see Fig. 23 and in the polarized case [47, 48, 49]. We show in Fig. 23 a comparison with MRST and CTEQ, where one observes that the essential differences lie in the small x region. We have also identified some physical observables and kinematic regions, where we can make definite predictions. In particular, let us recall a slow decreasing behavior of $d(x)/u(x)$ for $x > 0.6$, the fact that $\bar{d}(x)/\bar{u}(x)$ should remain larger than one for $x > 0.3$, the signs $\Delta\bar{u}(x) > 0$ and $\Delta\bar{d}(x) < 0$ and our choice for $\Delta G(x)$. All these are real challenges and we look forward to new precise experimental data in the future.

References

[1] C. Bourrely, F. Buccella and J. Soffer, Eur. Phys. J. C **23**, 487 (2002). For a practical use of these PDF, see www.cpt.univ-mrs.fr/∼bourrely /research/bbs-dir/bbs.html.

[2] A. Niegawa and K. Sasaki, Prog. Theo. Phys. **54**, 192 (1975); R.D. Field and R.P. Feynman, Phys. Rev. D **15**, 2590 (1977)

[3] C. Bourrely, F. Buccella and J. Soffer, Mod. Phys. Lett. A **18**, 771 (2003)

[4] C. Bourrely and J. Soffer, Phys. Rev. D **51**, 2108 (1995)

[5] C. Bourrely and J. Soffer, Nucl. Phys. B **445**, 341 (1995)

[6] R.S. Bhalerao, Phys. Rev. C **63**, 025208 (2001)

[7] C. Bourrely, F. Buccella and J. Soffer, in preparation

[8] K. Gottfried, Phys. Rev. Lett. **18**, 1154 (1967)

[9] New Muon Collaboration, M. Arneodo *et al.*, Phys. Rev. D **50**, R1 (1994) and references therein; P. Amaudruz *et al.*, Phys. Rev. Lett. **66**, 2712 (1991); Nucl. Phys. B **371**, 3 (1992)

[10] SMC Collaboration, B. Adeva *et al.*, Phys. Rev. D **58**, 112001 (1998)

[11] SLAC E155 Collaboration, P. L. Anthony *et al.*, Phys. Lett. B **493**, 19 (2000)

[12] Jefferson Lab Hall A Collaboration, X. Zheng *et al.*, Phys. Rev. Lett. **92**, 012004 (2004)

[13] COMPASS Collaboration, E.S. Ageev *et al.*, CERN-PH-EP/2005-001

[14] G. Bunce, N. Saito, J. Soffer and W. Vogelsang, Annu. Rev. Nucl. Part. Sci. **50**, 525 (2000)

[15] H1 Collaboration, C. Adloff *et al.*, Eur. Phys. J. C **30**, 1 (2003) [hep-ex/0304003]

[16] G.R. Farrar and D.R. Jackson, Phys. Rev. Lett. **35**, 1416 (1975)

[17] Hermes Collaboration, K. Ackerstaff *et al.*, Phys. Lett. B **464**, 123 (1999)

[18] Jefferson Lab Hall A Collaboration, X. Zheng *et al.*, [nucl-ex/0405006 v4], Phys. Rev. C (to appear)

[19] SLAC E143 Collaboration, K. Abe *et al.*, Phys. Rev. D **58**, 112003 (1998)

[20] FNAL E866/NuSea Collaboration, E.A. Hawker *et al.*, Phys. Rev. Lett. **80**, 3715 (1998); J.C. Peng *et al.*, Phys. Rev. D **58**, 092004 (1998); R.S. Towell *et al.*, Phys. Rev. D **64**, 052002 (2001)

[21] R.S. Towell, talk presented at HiX2004, Marseille 26-28 July 2004, AIP Conference proceedings vol.747, 2005, (Eds. C. Bourrely, Z.E. Meziani, J. Soffer) p.211

[22] J.D. Bjorken, Phys. Rev. **148** (1966), 1467; Phys. Rev. D **1**, 1376 (1970)

[23] HERMES Collaboration, A. Airapetian *et al.*, Phys. Rev. Lett. **92**, 012005 (2004)

[24] Z. Zhang, *'New insights into the proton structure with ep collider HERA'*, LAL 00-57 [hep-ph/0012249]

[25] H1 Collaboration, C. Adloff *et al.*, Eur. Phys. J. C **19**, 269 (2001) [hep-ex/0012052]

[26] ZEUS Collaboration, S. Chekanov *et al.*, Eur. Phys. J. C **21**, 443 (2001); Eur. Phys. J. C **28**, 175 (2003); Phys. Rev. D **70**, 052001 (2004) [hep-ex/0401003]; Eur. Phys. J. C **32**, 1 (2003) [hep-ex/0307043]

[27] ZEUS Collaboration, S. Chekanov *et al.*, Phys. Lett. B **539**, 197 (2002), Err. B **552**, 308 (2003) [hep-ex/0205091]

[28] G.P. Zeller *et al.*, Phys. Rev. Lett. **88**, 091802 (2002); G.P. Zeller, "A precise measurement of the weak mixing angle in neutrino nucleon scattering", Ph. D. thesis, Northwestern University, Illinois, 2002

[29] CCFR Collaboration, U.K. Yang *et al.*, Phys. Rev. Lett. **87**, 251802 (2001); U.K. Yang, Ph. D. Thesis, University of Rochester (2001)

[30] NuTeV Collaboration, D. Naples *et al.*, Proceedings from DIS03, St. Petersburg, Russia, April 2003; V. Radescu, XII International Workshop on Deep Inelastic Scattering, Slovakia (April 2004)

[31] NuTeVPack is available at www-nutev.phyast.pitt.edu/results_2004/nutev_sf.html

[32] FNAL E866/NuSea Collaboration, J.C. Webb *et al.*, submitted to Phys. Rev. Lett. [hep-ex/0302019]

[33] FNAL E605 Collaboration, G. Moreno *et al.*, Phys. Rev. D **43**, 2815 (1991)

[34] FNAL E772 Collaboration, P.L. McGaughey *et al.*, Phys. Rev. D **50**, 3038 (1994); D **60**, 119903 (1999)

[35] B. Jäger, M. Stratmann and W. Vogelsang, Phys. Rev. D **70**, 034010 (2004)

[36] CDF Collaboration, T. Affolder *et al.*, Phys. Rev. D **64**, 032001 (2001)

[37] D0 Collaboration, B. Abbott *et al.*, Phys. Rev. D **64**, 032003 (2001)

[38] D0 Collaboration, B. Abbott *et al.*, Phys. Rev. Lett. **86**, 1709 (2001)

[39] F. Aversa *et al.*, Nucl. Phys. B **327**, 105 (1989)

[40] J. Binnewies, B.A. Kniehl and G. Kramer, Z. Phys. C **65**, 471 (1995); Phys. Rev. D **52**, 4947 (1995)

[41] B.A. Kniehl, G. Kramer and B. Pötter, Nucl. Phys. B **582**, 514 (2000); B **597**, 337 (2001)

[42] PHENIX Collaboration, S.S. Adler *et al.*, Phys. Rev. Lett. **91**, 241803 (2003) [hep-ex/0304038]

[43] STAR Collaboration, G. Rakness, contribution to the XI Int. Workshop on Deep Inelastic Scattering (DIS2003), 23-27 April 2003, St. Petersburg, Russia; S. Heppelmann, contribution to the Transversity Workshop, 6-7 October 2003, IASA, Athens, Greece; J. Adams *et al.*, Phys. Rev. Lett. **92**, 171801 (2004) [hep-ex/0310058]

[44] C. Bourrely and J. Soffer, Eur. Phys. J. C **36**, 371 (2004)

[45] A.D. Martin *et al.*, Eur. Phys. J. C **35**, 325 (2004)

[46] J. Pumplin *et al.*, J. High Energy Phys. **0207**, 012 (2002)

[47] M. Glück, E. Reya, M. Stratmann and W. Vogelsang, Phys. Rev. D **63**, 094005 (2001)

[48] Y. Goto *et al.*, Phys. Rev. D **62**, 034017 (2000)

[49] E. Leader, A.V. Sidorov and D.B. Stamenov, Eur. Phys. J. C **23**, 479 (2002)